JOURNAL OF AIRCRAFT
Vol. 30, No. 6, Nov.–Dec. 1993

Optimization of Joined-Wing Aircraft

John W. Gallman* and Stephen C. Smith*
NASA Ames Research Center, Moffett Field, California 94035
and
Ilan M. Kroo†
Stanford University, Stanford, California 94305

The joined wing is an innovative aircraft configuration with a rear wing that has its root attached near the top of the vertical tail and a tip that sweeps forward to join the trailing edge of the main wing. This study demonstrates the application of numerical optimization to aircraft design and presents a quantitative comparison of joined-wing and conventional aircraft designed for the same medium-range transport mission. The computer program developed for this study used a vortex-lattice model of the complete aircraft to estimate aerodynamic performance, and a beam model of the lifting-surface structure to calculate wing and tail weight. Weight estimation depended on a fully stressed design algorithm that included a constraint on buckling and a correlation with a statistically based method for total lifting-surface weight. A variety of "optimum" joined-wing and conventional aircraft designs are compared on the basis of direct operating cost, gross weight, and cruise drag. Maximum lift and horizontal tail buckling were identified as critical joined-wing design issues. The addition of a buckling constraint is shown to decrease the optimum joined-wing span and increase direct operating cost by about 4%. The most promising joined-wing designs were found to have a joint location at about 70% of the wing semispan, a fuel tank in the tail to trim, and a flap spanning 70% of the wing. These designs are shown to cost 3% more to operate than a conventional configuration designed for the same medium-range mission.

Nomenclature

A_{min} = minimum gauge cross-sectional area of stringer, in.^{2}
A_1, A_2 = cross-sectional area of stringer shown in Fig. 4, in.^{2}
b_t = tail span measured in plan view, ft
b_w = wing span measured in plan view, ft
C_{MAC} = wing mean aerodynamic chord, ft
C_x = half-chord dimension of beam cross section, ft
C_z = half-thickness dimension of beam cross section, ft
E = Young's modulus, lb/in.^{2}
F_x = structural shear load applied in local x direction (see Fig. 4), lb
F_y = beam tensile load (see Fig. 4), lb
F_z = structural shear load applied in local z direction (see Fig. 4), lb
G = torsional modulus, lb/in.^{2}
I_t = lift-dependent tail weight index
I_w = lift-dependent wing weight index
I_{xx}, I_{zz} = area moments of inertia of beam cross section, in.^{4}
I_{xz} = product of inertia for beam cross section, in.^{4}
J = polar moment of inertia, in.^{4}
l_t = tail arm or distance between aircraft c.g. and tail aerodynamic center ft
M_x, M_y, M_z = moments applied about local axis system of beam cross section, in.-lb
n = ultimate load factor
S_{ls} = area of a lifting surface, ft^2
S_t = area of tail, ft^2
S_w = area of wing, ft^2
T_{min} = minimum gauge skin thickness
T_x = skin thickness of beam cap, in.
T_z = skin thickness of beam web, in.
$(t/c)_{ave}$ = average thickness-to-chord ratio
u = transverse deflection of beam section in local coordinates, in.
W_{ls} = total weight of lifting surface, lb
W_{min} = minimum gauge structural weight, lb
W_{str} = structural weight, lb
W_t = tail weight, lb
W_{TO} = aircraft maximum takeoff weight, lb
W_w = wing weight, lb
W_{ZFW} = aircraft zero fuel weight, lb
w = vertical deflection of beam section in local coordinates, in.
x, y, z = local beam coordinates shown in Fig. 4
θ = rotational deflection of beam section in local coordinates, rad
Λ_{EA} = sweep angle of the elastic axis
λ = wing taper ratio, tip chord/root chord
σ_a = allowable tensile stress, lb/in.^{2}
τ_a = allowable shear stress, lb/in.^{2}

Introduction

THE joined wing is an innovative aircraft configuration with a rear wing that has its root attached near the top of the vertical tail and a tip that sweeps forward to join the trailing edge of the main wing (see Fig. 1). The rear wing (or tail) is used both for pitch control and as a structural support for the forward wing. When compared with a conventional wing-tail configuration, several advantages have been predicted for joined wings. The potential for lower structural weight and less drag are probably the most important of these advantages. Joining the tail to the wing allows the tail to act

Received Jan. 2, 1992; revision received Aug. 15, 1992; accepted for publication Sept. 2, 1992.

*Aerospace Engineer, M/S 227-2. Member AIAA.
†Associate Professor, Department of Aeronautics and Astronautics. Member AIAA.

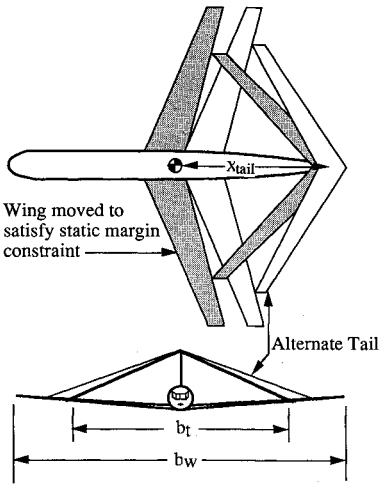

Fig. 1 Typical joined-wing aircraft with two alternate tails.

as a strut, relieving wing bending moments inboard of the wing-tail joint. Because these lifting surfaces are nonplanar, a reduction in induced drag is also suggested by Ref. 1.

Wolkovitch[2,3] first proposed the joined-wing concept in 1976, and has studied its application to supersonic fighters, long endurance platforms, and commercial transports. The fundamental structural and aerodynamic characteristics of joined wings have been studied by several researchers. Joined wings were shown to be significantly lighter than cantilever wing structures in Refs. 4 and 5. Hajela's[6] study of joined-wing structures indicated the importance of in-plane loads, and suggested that nearly rigid joint structures were best. Letcher's[7] aerodynamic analyses showed that optimally loaded joined wings with tip joints have less induced drag than conventional wings of the same span. Kroo et al.[8] used a vortex-lattice code and a structures routine based on inextensible beam theory to compare the cruise drag of joined wings with conventional designs of the same lifting-surface area and structural weight. This study showed a savings of 11% in cruise drag for a joined wing with a joint located at about 70% of the wing semispan.

Although this reduction in cruise drag is significant, consideration of all the flight conditions required for a particular mission is needed to demonstrate any economic savings for joined wings. Performance constraints such as takeoff field length, landing field length, and climb gradient could increase the wing area required for a joined-wing configuration, thereby eliminating potential drag reduction. Several programs[9,10] evaluate aircraft performance at many flight conditions and estimate economic efficiency, but neither the structures nor aerodynamics are represented in sufficient detail for an accurate evaluation of joined-wing aircraft.

The goals of this study are to demonstrate the application of numerical optimization to aircraft design and to present a quantitative comparison of joined-wing and conventional aircraft designed for the same medium-range transport mission. A computer program capable of modeling joined-wing aircraft and estimating their overall performance in terms of direct operating cost (DOC) was developed. This program performs aerodynamic and structural analyses that are significantly more sophisticated than those used in most preliminary design codes. This sophistication is needed to predict the aerodynamic interference between the lifting surfaces and the stresses in the statically indeterminate structure. First, a vortex-lattice model of the complete aircraft is used to calculate aerodynamic forces. These calculations are performed using a subroutine version of the LinAir[11] program. Viscous and compressibility drag are added to the vortex drag estimated by LinAir to calculate total transonic drag. Second, inextensible beam theory is used in a fully stressed design algorithm that includes a constraint on tail buckling. The structural design algorithm considers one maneuver load case, several gust load cases, and the nonlinear effects of secondary bending moments. The computed structural weight is then correlated with the results of a statistically based method[12] to obtain estimates of the total lifting-surface weight. Finally, the numerical optimizer, NPSOL,[13] is used to design joined-wing and conventional transports with minimum DOC. This article describes the analysis methods used in the design code, discusses some problems encountered when applying the numerical optimizer, and compares optimum joined wings with conventional aircraft on the basis of cruise drag, lifting-surface weight, and DOC.

Analysis Methods

Aircraft optimization requires computational methods that quickly evaluate aircraft performance characteristics for a wide range of geometric configurations and flight conditions. The development of analysis methods for joined-wing aircraft design focused on the interaction between trimmed drag and structural weight. The methods used to calculate the aerodynamic load distributions, the total aircraft drag, and the weight of the aircraft components are described in the following sections. Integration of these analysis methods into the aircraft synthesis code and the application of NPSOL to the aircraft design problem are also discussed.

Aerodynamic Modeling

Aerodynamic forces are calculated in the design code using a subroutine version of the LinAir program. This subroutine solves the Prantl-Glauert equation using a vortex-lattice method and calculates induced drag using Trefftz-plane integration. Vortex-lattice models of the lifting surfaces, the lifting surfaces plus fuselage, and the complete aircraft with engines and pylons were considered. A complete aircraft model was necessary to accurately represent the downwash on the tail, and therefore, the tail's contribution to the static margin. Wings were modeled using two spanwise elements with linear twist distributions. These two elements allow for a discontinuity in twist and span wing sections inboard and outboard of the joint. This discontinuity produced joined wings with slightly less trimmed drag than those with linear twist distributions from root to tip. This reduction in drag indicates that a discontinuity in wing twist enables the aircraft to generate a more elliptic load distribution. A third wing element represented the flapped portion of the wing. Tails were modeled as one spanwise element with a linear twist distribution. An example vortex-lattice model and lift distributions for both the wing and tail are shown in Fig. 2. This figure shows that the aerodynamic modeling is sophisticated enough to represent changes in the wing's lift distribution due to flap deflection and changes in the tail's lift distribution due to elevator deflection.

For computational efficiency, the aerodynamic forces at many different flight conditions are represented as a linear

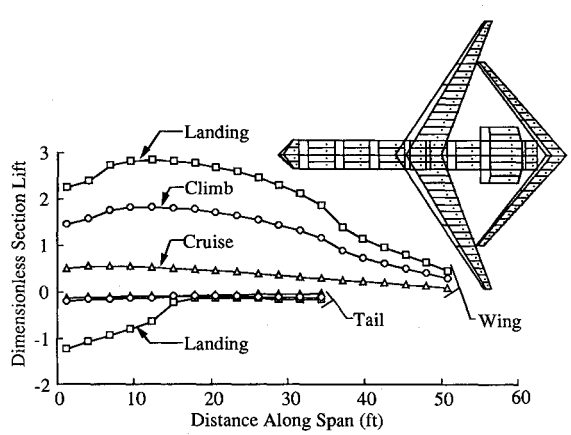

Fig. 2 Wing and tail lift distributions for a typical joined wing that is trimmed for climb, cruise, and landing approach.

combination of four solutions to the vortex-lattice problem. The first of the four solutions is for the complete aircraft model at an angle of attack equal to zero. The three remaining solutions represent independent perturbations in angle of attack, wing incidence, and tail incidence. The influence coefficients required to represent the aerodynamic forces as a sum of these four solutions need to be evaluated whenever the size, shape, or spatial orientation of the lifting surfaces are changed. Since only a few design variables cause these changes, many design modifications can be investigated without additional solutions of the vortex-lattice problem. Additional computational time is saved by assuming the aerodynamic influence coefficients are constant with respect to small changes in panel incidence, and by evaluating all the aerodynamic forces at a Mach number of 0.5. This is an excellent approximation in the aerodynamic influence coefficients, since the change in freestream flow normal to the panel is primarily responsible for any change in bound vortex strength associated with variations in incidence. A Mach number of 0.5 is small enough for low-speed flight and simple corrections are used to obtain loads at higher subsonic Mach numbers.

Values for the aircraft maximum lift coefficient are determined using a method (similar to that of Ref. 14) based on flight test data, wind-tunnel data, and vortex-lattice calculations. An equation for wing maximum lift[15] is developed by comparing vortex-lattice calculations with experimental data for a family of transport wings with different airfoil sections and sweep angles. Section lift coefficients are calculated by the vortex-lattice method at a series of increasing wing angles of attack. The wing maximum lift is obtained when any calculated section lift coefficient reaches its experimental maximum. Corrections are made to this basic value to account for flap deflection, slat deflection, and Mach number. The contribution of the tail loads required to trim are then included to calculate the aircraft's maximum lift.

Drag calculations in this study are divided into three major categories: 1) vortex-induced drag, 2) viscous drag, and 3) compressibility drag. The vortex drag is calculated using LinAir at a Mach number of 0.5 for trimmed flight in both cruise and climb. Since the complete aircraft and its wake are modeled, this vortex drag includes trim drag and inviscid interference drag. Lift-dependent viscous drag is assumed to vary parabolically with lift for each airfoil section ($0.003C_l^2$). This relationship represents the variation in minimum section drag with design lift coefficient and assumes the airfoils are cambered for best cruise performance. Section drag values calculated from the corresponding section lift are integrated over the wing span and the tail span to obtain the total lift-dependent viscous drag for the lifting system. An empirical relationship based on flight test data of modern transport aircraft accounted for all other contributions, primarily caused by viscous interference, to lift-dependent viscous drag. Viscous drag that is independent of lift is calculated using exposed wetted areas and the von Kármán formulas for the skin friction drag of a flat plate.[16] Corrections are made to these drag calculations to account for surface roughness.[17] Other viscous drag items such as control surface gap drag and nacelle base drag are also treated explicitly. The compressibility drag is defined here as all the drag caused by an increase in Mach numbers above 0.5. This drag increment is a function of airfoil thickness-to-chord ratio, section lift coefficient, wing sweep, and Mach number. It is computed using the methods of McGeer and Shevell.[18]

Structures and Weight Prediction

The weight of an aircraft wing depends strongly on its applied loads. Federal Aviation Regulations Part 25 (FAR 25) prescribe many more load cases than can be practically considered in an aircraft optimization code. The flight envelope prescribed by these loads is defined by gust and maneuver diagrams. Structural design and weight prediction was performed for several flight conditions to determine the most critical load cases and to select a minimum subset. The gust loads are calculated at the flight speeds V_B and V_C, defined in FAR 25 for the gust diagram. Because the cruise Mach number is held constant, V_C is approximately equal to 350 kt equivalent airspeed and V_B (see FAR 25) is less than V_C. Positive and negative gusts at 20,000 ft of 66 ft/s at V_B and 50 ft/s at V_C (equivalent airspeeds) define the gust load cases. A 2.5 g maneuver load at the design dive speed V_D, selected to be $1.15V_C$, is also considered.

Joined-wing structures carry loads very differently from conventional cantilever wing structures. This difference makes the lifting-surface weight prediction more difficult for joined wings than for conventional aircraft. Connecting the tail to the wing causes reaction forces that relieve wing bending moments inboard of the joint. Figure 3 shows this bending moment relief for bending moments caused by both positive and negative gusts. This interaction between the wing and tail causes the material stress distributions to depend on structural stiffness. Since conventional wing structures do not have this characteristic, weight estimation methods based on existing airplanes are inadequate for joined wings. One alternative is to design the load-carrying structure and calculate the structural weight. But the wing structure required to support the flight loads represents only about 60% of the total wing weight. Minimum-gauge structure, control systems, and fuel systems make up the remaining wing weight. Therefore, a correlation was used to predict total wing weight from calculated structural weight.

The wing and tail structures are modeled with skin-stringer beams as shown in Fig. 4. Both beams are cantilevered at the root, and the joined-wing joint structure is assumed to be rigid, as suggested in Ref. 19. As described in Ref. 3, the resultant bending moment tends to be oriented diagonally across the structural box because the reactions at the wing-tail joint cause significant forces in the plane of the wing. The asymmetric distribution of material shown in Fig. 4 enables

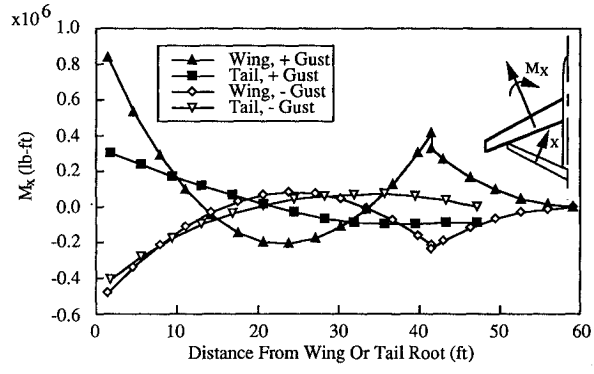

Fig. 3 In-plane, or M_x bending moment distributions for a typical joined wing subjected to both positive and negative gust loads.

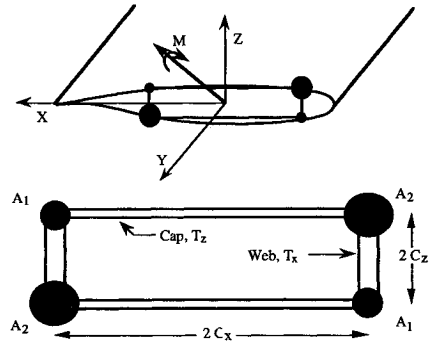

Fig. 4 Structural box model with skins, stringers, and the resultant bending moment.

the joined-wing structure to resist this bending moment efficiently. Figure 4 also defines the stringer areas A_1 and A_2, the web and cap thicknesses T_x and T_z, and the structural box dimensions C_x and C_z. C_x and C_z are calculated as a function of spar width so that the box fits into the airfoil section, and A_1, A_2, T_x, and T_z are treated as structural design variables. Sections of the wing outboard of the joint and all conventional designs use structural boxes that extend over the thickest 20% of the airfoil section. Although this modeling neglects shear lag, results from earlier studies indicate such effects are negligible for the high-aspect ratio structures studied here.[20]

The structural analysis method is based on inextensible beam theory. This theory represents the wing and tail deflections as the solution of the following ordinary differential equations:

$$\frac{d^2w}{dy} = \frac{M_x I_{zz} + M_z I_{xz}}{E(I_{xx}I_{zz} - I_{xz}^2)} \tag{1}$$

$$\frac{d^2u}{dy} = \frac{-(M_z I_{xx} + M_x I_{xz})}{E(I_{xx}I_{zz} - I_{xz}^2)} \tag{2}$$

$$\frac{d\theta}{dy} = \frac{M_y}{GJ} \tag{3}$$

Here w, u, and θ are vertical, transverse and rotational deflections respectively, and M_z, M_x, and M_y are the corresponding applied moments. Structural box dimensions and material thicknesses give the inertia terms in Eqs. (1–3) as

$$I_{xx} = 2(A_1 + A_2)C_z^2 \tag{4}$$

$$I_{zz} = 2(A_1 + A_2)C_x^2 \tag{5}$$

$$I_{xz} = 2(A_1 - A_2)C_xC_z \tag{6}$$

$$J = \frac{16C_x^2C_z^2T_xT_z}{C_xT_x + C_zT_z} \tag{7}$$

The deflection equations [Eqs. (1–3)] are used to construct a matrix of structural influence coefficients describing the effect of unit joint-reaction forces and moments on joint rotations and deflections. The joint-reaction forces are then determined by requiring zero relative deflection between the tail tip and the wing joint. This analysis produces a deflection distribution and a set of joint reactions that are caused by the applied loads or primary bending moments only. Once the structure deflects, axial reaction forces produce secondary bending moments that can cause an increase in maximum deflection or failure due to buckling.

Secondary bending moments are included in the structural analysis by adding them to the applied loads [M_x, M_y, and M_z in Eqs. (1–3)]. Since these secondary moments are dependent on the deflected shape, the solution for the joint reactions begins with an estimate of the deflection distribution and proceeds iteratively until the input and output deflections are the same. Updates of the deflection distribution are underrelaxed by 0.2 for load cases that produce tensile tail loads and 0.7 for load cases that produce compressive tail loads. Equations (1–3) are based on the assumption of small deflections, and therefore, cannot be expected to give an accurate representation of large deflections. However, this analysis method proved quite useful for determining if tail buckling was a problem and for designing tail structures that are free from a buckling instability. Figure 5 shows a front view of the two primary buckling mode shapes for joined-wing structures and the increase in deflection with iterative updates of the secondary bending moments. Since the input and output deflections have not converged, Fig. 5 also demonstrates that buckling is a design issue for some joined-wing structures.

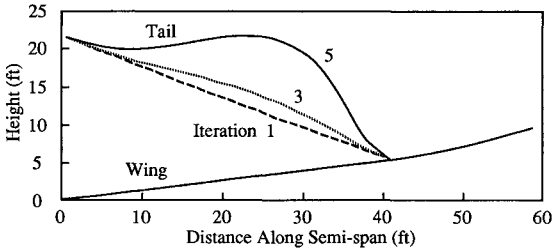

a) Mode shape number 1

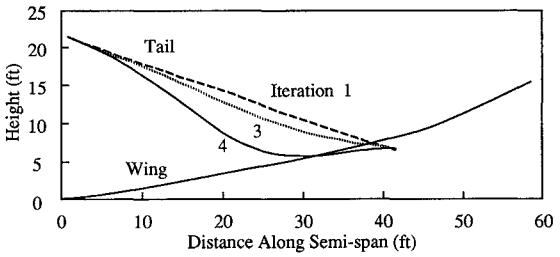

b) Mode shape number 2

Fig. 5 Front view of the two primary buckling mode shapes for joined-wing structures and the increase in deflection with iterative updates of the secondary bending moments. The joint structure has been left out for clarity.

The joint reactions, applied loads, and secondary bending moments were used to design the lifting structures that are approximately fully stressed. Additional material must be added to the fully stressed distribution to avoid buckling. Using a structural design method, rather than optimizing the structure and aircraft configuration simultaneously, reduced the number of optimization variables by about 200 and simplified the numerical optimization problem. Since stress depends on stiffness in joined wings, a fully stressed structure is likely to be slightly heavier than an optimum structure. However, we considered these structures close enough to minimum weight to justify comparing joined wing and conventional transport performance. Figure 4 shows the asymmetric material distribution that yields a fully stressed design for joined wings. This distribution of material is determined by solving the stress equations for member thickness. The shear stress equations are rearranged to give the fully stressed skin thicknesses as

$$T_x = \frac{2|F_z|C_x + |M_y|}{8\tau_a C_x C_z} \tag{8}$$

$$T_z = \frac{2|F_x|C_z + |M_y|}{8\tau_a C_x C_z} \tag{9}$$

where τ_d is the allowable shear stress, F_x and F_z are shear loads, and M_y is an applied torque. Setting the stress in each of the stringers A_1 and A_2 equal to the allowable stress (σ_a) produces a set of quadratic equations for A_i in terms of A_j given by

$$A_1^2 + \left[A_2 - \left(\frac{|F_y|}{2\sigma_a} + \frac{|M_xC_x - M_zC_z|}{4C_xC_z\sigma_a}\right)\right]A_1 - \frac{|M_xC_x - M_zC_z|}{4C_xC_z\sigma_a}A_2 = 0.0 \tag{10}$$

$$A_2^2 + \left[A_1 - \left(\frac{|F_y|}{2\sigma_a} + \frac{|M_xC_x + M_zC_z|}{4C_xC_z\sigma_a}\right)\right]A_2 - \frac{|M_xC_x + M_zC_z|}{4C_xC_z\sigma_a}A_1 = 0.0 \tag{11}$$

where F_y is the tensile load, and M_x and M_z are the bending moments. These equations can be decoupled by assuming that the stress in A_1 is equal to the stress in A_2. However, this assumption is violated when a minimum gauge constraint is active. Since stringer areas of zero would produce zero bending inertia and cause Eqs. (1) and (2) to become indefinite, a minimum gauge constraint given by

$$A_{\min} = (C_x + C_z)T_{\min} \tag{12}$$

and $T_{\min} = 0.04$ in. is enforced during structural sizing calculations. Equation (12) forces a lightly loaded element to have enough minimum gauge skin to define the shape of the structural box. This minimum gauge constraint is applied after the positive roots of Eqs. (10) and (12) are used to size the stringers. Obviously, the value of A_2 used in Eq. (10) and the value of A_1 used in Eq. (12) correspond to a previous sizing iteration. The need for an iterative structural design procedure is produced by the dependence of the joint reactions on material thickness, even when secondary bending moments are ignored.

Multiple load cases are considered in five steps:

1) A single material distribution and an appropriate deflection distribution for each load case are chosen based on previous design results or prescribed initial distributions.

2) The joint reactions are calculated for each load case using one structural analysis iteration (deflections are not converged). This analysis iteration produces a new deflection distribution for each load case.

3) A material distribution is calculated for each load case using Eqs. (8–12).

4) The maximum thickness is chosen for each member from the material distributions calculated in step 3.

5) Material and deflection distributions are updated and the procedure returns to step 2 until the structural weight of the wing and of the tail change by less than a prescribed tolerance.

This design method typically takes 25–30 iterations to converge to the precision required for the gradient optimization.

Modifications to the design load cases were required to produce structures that were stable with respect to both of the buckling mode shapes shown in Fig. 5. This load modification forces the design algorithm to add material to the fully stressed distribution. Wing loads were increased by 2400 lb, and the number of design load cases was doubled by both increasing and decreasing the tail load by about 100 lb. The extra wing load was applied as a percentage increase to the specified distribution, and the extra tail load was distributed in a half sine wave centered about the tail's semispan. Without these modifications, the method could produce a structure whose design load was equal to the critical buckling load of one mode shape. *Decreasing* the loads (or safety factor) for this structure created buckling in the other mode shape. The small increments in tail load were chosen to force the design method to consider both mode shapes shown in Figs. 5a and 5b without adding unnecessary weight. This increment in tail load was most important when the design tail loads were small or zero, because relatively large positive or negative tail loads would force a particular buckling mode shape. Once a structural design is completed using the above method, buckling stability is checked by perturbing the deflection distribution and verifying that the structure returns to its equilibrium shape. The local deflections were increased or decreased by 10% when perturbing the structure. Figure 5 shows how the secondary bending moments create an increase in deflection for a structure that is unstable in either mode 1 or mode 2.

The current weight method was developed using calculated structural weight and the results of a statistically based weight method similar to that of Ref. 12. Reference 12 estimates the lift-dependent wing weight and the lift-dependent tail weight using

$$I_w = \frac{nb_w^3\sqrt{W_{\text{TO}}W_{\text{ZFW}}}(1 + 2\lambda)}{(t/c)_{\text{ave}}\cos^2(\Lambda_{\text{EA}})S_w^2(1 + \lambda)} \times 10^{-6} \tag{13}$$

$$I_t = \frac{nb_t^3W_{\text{TO}}C_{\text{MAC}}}{1.875(t/c)_{\text{ave}}\cos^2(\Lambda_{\text{EA}})l_tS_t^2} \times 10^{-6} \tag{14}$$

Equations (13) and (14) relate the applied loads, geometric shape, and load-dependent weight. The overall wing and tail weights are then given by a linear fit to data available for a variety of transport aircraft

$$W_w = (1.64I_w + 4.25)S_w \tag{15}$$

$$W_t = (1.5I_t + 5.0)S_t \tag{16}$$

where the second term in these equations accounts for minimum gauge structure and system components that are independent of load. Figures 6 and 7 present the wing and tail weights for these production aircraft and the linear fits defined in Eqs. (15) and (16). Since Eqs. (13) and (14) were developed for conventional configurations, they do not capture the structural interaction between the wing and tail of a joined wing.

The relationship between loads, shape, and total weight is captured in the current weight method by designing a structure for a particular configuration, which is subjected to critical flight loads. Calculated structural weight then replaces I_w and I_t in the current method. Lifting-surface weight is calculated using

$$W_{\text{ls}} = 1.35(W_{\text{str}} - W_{\min}) + 4.9S_{\text{ls}} \tag{17}$$

where W_{str} is the total calculated structural weight of the lifting surface and $W_{\min}$ is the structural weight of the lifting surface when all elements are at minimum gauge. Equation (17) also

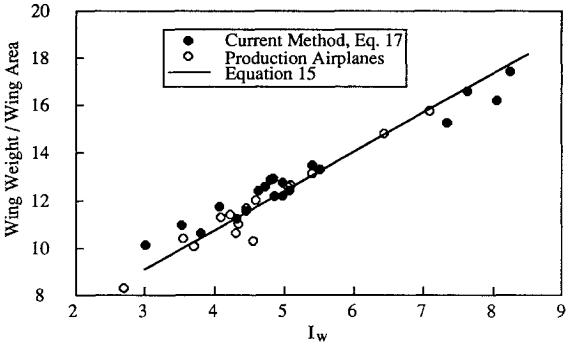

Fig. 6 Comparison of wing weight prediction with actual production airplanes and weight estimates performed using the method of Ref. 12.

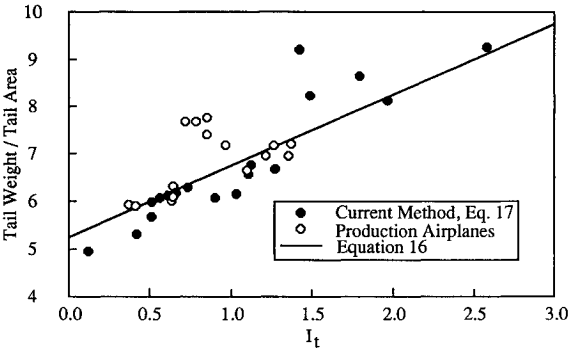

Fig. 7 Comparison of tail weight prediction with actual production airplanes and weight estimates performed using the method of Ref. 12.

represents a linear fit of data for existing transport aircraft. The numbers 1.35 and 4.9 that define this fit were determined by comparing weight estimates from Eq. (17) with estimates from Eqs. (15) and (16).

The geometric data necessary to design structures for each of the production aircraft in Figs. 6 and 7 was not available, making a direct comparison of the current weight method with actual aircraft weights impossible. The accuracy of the current method was tested by estimating the weights of a family of proposed wings and tails that span a range of values for I_w and I_t. These weights were then compared with the results of Eqs. (15) and (16), which are shown to produce acceptable weight estimates for actual production aircraft in Figs. 6 and 7. These figures also show good agreement between the two weight prediction methods and indicate the scatter in the weights of the production aircraft.

Optimization

Aircraft optimization problems with 17 variables, 9 mission constraints, and bound constraints on each variable were solved successfully in this study. The aircraft synthesis code is general enough to allow for a much larger selection of design variables, but this set was considered sufficient to provide a realistic comparison of joined-wing and conventional aircraft performance. Table 1 lists the design variables, key parameters that were fixed during the optimization, and some performance results for a few conventional and joined-wing configurations. Explicit nonlinear constraints simplified the synthesis code by eliminating the iteration loops commonly found in many other design codes.[9,10] A combination of experimental and flight test data available for the McDonnell Douglas DC-9-30[21] was used to verify the accuracy of the design code at estimating aircraft performance. For example, estimated values for cruise drag were within a few percent of those measured in flight test. One test of the design code was conducted by optimizing a conventional transport for the same mission as a DC-9-30. This study indicated that a DC-9-30 is nearly optimum for its intended mission. Direct operating cost for a medium-range transport mission was used as the objective function. It was evaluated using a modified version of the 1967 ATA standard method of estimating comparative operating costs of turbine powered aircraft.[22] This method includes estimates of crew, maintenance, depreciation, fuel, and insurance costs. The mission requirements are to transport 115 coach passengers 2000 n.mi. at a cruise Mach number of 0.78. All designs have a stick-fixed static margin of 0.2 based on a reference chord of 13.69 ft. A balanced runway length of 7800 ft at sea level is used for the takeoff and landing field length constraints. Other constraints include an engine-out climb gradient greater than 2.4%, a cruise thrust greater than cruise drag, and cruise trim at cruise lift coefficient. The trim constraint is enforced at an average cruise weight. Trimming moments required for other weights or flight conditions are generated by deflecting the elevator. Sufficient pitch control for takeoff rotation is also required.

NPSOL, a gradient-based optimizer, uses a sequential quadratic programming algorithm to solve the design problem. This algorithm solves a quadratic subproblem to determine the appropriate search direction in design space, performs a line search in this direction, and minimizes an augmented Lagrangian merit function.[23] Figure 8 shows convergence of the objective function and the constraint function violations for a typical 17 variable, 9 constraint problem. This figure shows convergence to an optimal design in 500 s of computational time on a Cray Y-MP. Including secondary bending moments in the structural design algorithm increased this computational time by approximately a factor of 10.

Two interesting problems were encountered during application of numerical optimization to the design problem. The first problem was associated with an inaccurate calculation of induced drag caused by a discontinuity in the panel width

Table 1 Joined-wing design variables, fixed parameters, and optimum solutions

	Conventional		Joined wing		
	Ref.	Best	case 1	case 2	case 3
Design variables					
Wing area	1,127.6	1,013.3	1,282.3	1,288.9	1,024.1
Wing span	101.2	98.8	117.3	107.7	104.4
Wing root incidence	5	4.8	7.2	6.9	6.9
Inboard joint incidence	5.5	5.4	3.8	5.3	5.1
Outboard joint incidence	5.3	5.3	4.6	3.8	6.1
Wing tip incidence	1.8	1.9	1.8	1.4	1.6
Average wing, t/c	0.12	0.12	0.10	0.10	0.09
Longitudinal wing position	58.3	56.4	61.3	63.6	61
Tail area	225	225	314.5	512.6	459.7
Tail root incidence	0.42	2.5	−2	0.5	1.4
Tail tip incidence	1.2	1.7	3	1.8	4.3
Average tail, t/c	0.11	0.11	0.16	0.16	0.16
Static thrust per engine	17,525	17,262.5	17,008.5	18,231.1	18,136.7
Initial cruise altitude	32,806.7	32,274.9	38,242.5	37,706.5	37,826.8
Final cruise altitude	34,516.4	34,015.5	39,849.5	39,336.6	39,354.6
Takeoff flap deflection	10.5	11.2	22.7	18.8	21.8
Fixed parameters					
Wing sweep	30	30	30	30	30
Wing dihedral	6	6	6	6	6
Wing structural box chord	0.5	0.5	0.5	0.5	0.5
Tail sweep	32	32	−33.2	−34.9	−37.4
Tail dihedral	−3	−3	−23.1	−25.4	−26.2
Tail structural box chord	0.5	0.5	0.5	0.5	0.5
Flap span/wing span	0.5	0.7	0.5	0.5	0.7
Elevator span/wing span	0.4	0.4	0.7	0.7	0.4
Performance results					
W_{TO}	130,068.6	127,891.1	133,491.6	137,266.0	132,294.5
Fuel tank for trim	No	Yes	No	No	Yes
Buckling constraint	n/a	n/a	No	Yes	Yes
Relative cruise drag	1.000	0.982	0.958	1.051	0.994
Relative DOC	1.000	0.986	1.006	1.048	1.018

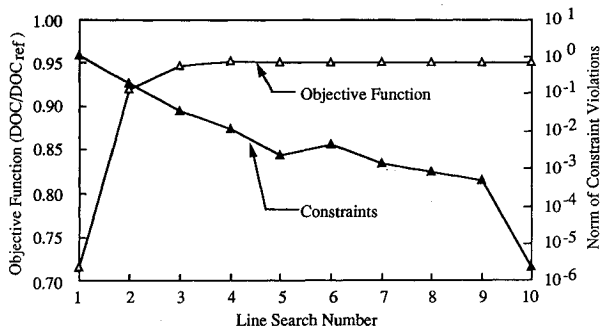

Fig. 8 Iteration history of the objective and constraint violations for a joined-wing optimization problem.

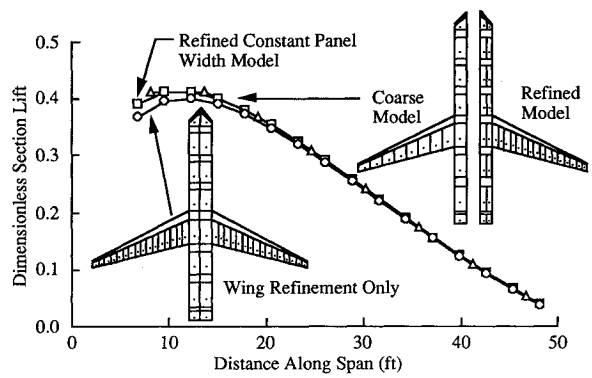

Fig. 9 Lift distributions calculated with and without a panel discontinuity at the wing-fuselage joint.

used in the vortex-lattice model. This caused the numerical optimizer to suggest that unrealistic wing twists were optimum. Figure 9 shows two lift distributions calculated using wing-fuselage models with constant panel widths and a third model with a discontinuity in panel width at the wing fuselage joint. Although the panel discontinuity is exaggerated in Fig. 9, a difference of 10% in panel width produced significant errors in the twist distributions of optimum solutions. Realistic solutions were obtained by introducing some vertical separation between wing and fuselage models and fixing the number of wing panels. With this modeling, wing span could be treated as a continuously differentiable variable. However, tail span had to be varied parametrically, since it was defined by an integer number of wing panels. The second problem was lack of function smoothness. Very smooth functions were required for reliable application of the design code. Furthermore, precise knowledge of function smoothness was necessary for the appropriate choice of finite difference step sizes and the choice of convergence criteria for the optimization problem. A numerical method designed to estimate round-off error[24] was found to be invaluable at identifying the sections of an analysis algorithm that were responsible for non-smooth or discontinuous function behavior and for estimating function smoothness.

Results

All joined-wing design results are compared with similarly designed conventional T-tail aircraft on the basis of drag, weight, and DOC. The DC-9-30 represented the baseline configuration for the conventional transports. Drag, weight, and DOC are all normalized with respect to values calculated for the optimized conventional transport labeled Ref. in Table 1. Since the Pratt and Whitney JT8D-9 low bypass ratio engine was used on the DC-9-30, a "variable-size" version of this engine is used throughout this design study. All estimates of DOC assume that the cost of jet fuel is 70 cents/gal.

Tail-to-wing span ratio was shown to be an important design variable in Ref. 8. Since both the wing and the tail could not be modeled with an integer number of constant width panels, span ratio was studied parametrically. This parametric study showed very little change in DOC for values of tail-to-wing span ratio (b_t/b_w) between 0.6–0.8. The small variation in DOC from $b_t/b_w = 0.6$ to $b_t/b_w = 0.8$ corresponded to a decrease in the optimum wing span of 5%. As suggested in Ref. 8, the optimum tail-to-wing span ratio was 0.7. Since Ref. 8 considered only a single design point, a cruise condition, it is interesting that the operational constraints considered in this study do not affect the choice of span ratio for joined wings.

A parametric study of wing span was performed to estimate the sensitivity in DOC, and as a check on optimality with respect to this crucial design variable. As expected, the optimum span for both joined-wing and conventional transports represents a compromise between increasing weight and decreasing drag. Figure 10 shows this trade-off between gross weight and average cruise drag for both conventional and joined-wing configurations. This figure shows joined-wing designs are inferior by 4% in weight and 7% in drag at fixed span. At fixed weight, the conventional configuration has a much longer wing span. Comparing joined-wing and conventional configurations with optimum span shows an increase of about 5.5% in both weight and drag for the joined wing. These results are opposite to those of Ref. 8, because the joined wing needs a larger wing to satisfy the takeoff field length requirement and a larger tail with more structural material to prevent buckling. Figure 11 emphasizes the importance of aft tail buckling by presenting the DOC of joined wings designed with and without a buckling constraint. Any standardized cost model cannot be expected to estimate the DOC accurately for a particular airline.[25] However, the trends in DOC agree with those presented for weight and drag in Fig. 10. Figure 11 shows that changing wing span from the optimum by 12–14% leads to an increase of about 1% in DOC. Both the set of optimum results which treat wing span

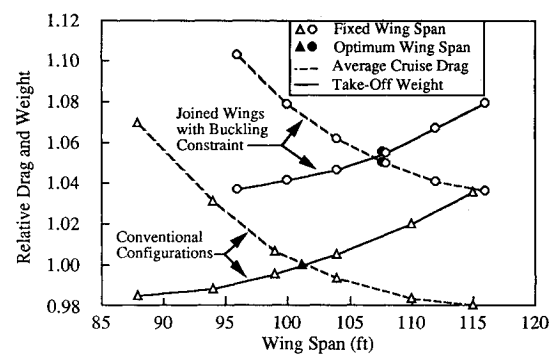

Fig. 10 Design tradeoff between cruise drag and gross weight for both conventional and joined-wing transports.

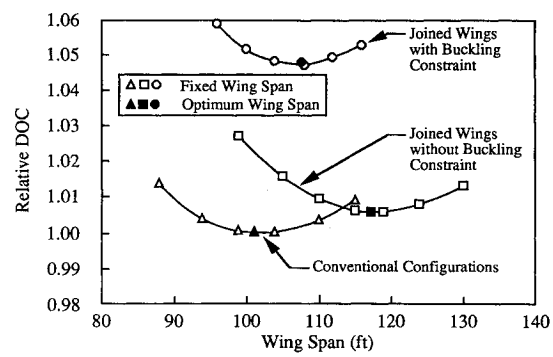

Fig. 11 Comparison of conventional transports with joined wings designed with primary bending moments only and with secondary bending moments.

as a fixed parameter and the results which include it as a design variable agree on the best value, indicating convergence of the optimization problem with respect to span. The best conventional and joined-wing designs presented in Fig. 11 are listed as Ref., case 1 and case 2 in Table 1. Overall, Fig. 11 shows that the joined wings analyzed here are about 5% more expensive to operate than a conventional configuration and that they suffer a penalty of approximately 4% for buckling.

A more careful investigation of the importance of design constraints is presented in Fig. 12. This figure illustrates five different design problems, all of which include constraints on range, cruise thrust, trim, and stability. Landing field length is an inactive constraint with no noticeable effect on the optimum design. The first set of bars in Fig. 12 present a comparison of joined wings with conventional aircraft designed for a cruise condition only. Problem 2 adds a takeoff field length constraint to this basic design problem and problems 3–5 each include the effects of an additional constraint.

In the cruise problem, the joined wing is shown to perform better than the conventional configuration. When the takeoff field length constraint is added in problem 2, the joined wing experiences a much larger increase in DOC. In contrast, when the constraint on climb gradient is added in problem 3, the joined wing has a smaller relative increase in DOC. This is a result of the joined wing's structural efficiency, but poor high-lift capability. The joined wing suffers a substantial penalty in maximum lift because of a short tail moment arm and the corresponding large tail download required to trim in takeoff configuration. This penalty forces the joined-wing aircraft to have a much larger wing, which increases the cruise drag and the operational costs. However, the strut-braced structure still has a longer wing span than the conventional configuration. This extra wing span reduces the induced drag during climb and makes it easier for the joined wing to satisfy the climb constraint. Reducing the penalty associated with the takeoff field length is the key to improving the optimal joined wing. Moving the mass center of the empty aircraft forward, thereby reducing the operational range of mass center, and designing to a lower level of static stability are obvious ways to reduce this penalty. Passenger and baggage accommodations make major changes in mass center location impractical. However, redistributing the fuel and locating the engines on the wing could have a significant impact on takeoff field length. The resulting effect on overall performance could make the joined-wing DOC less than that of the conventional configuration, especially since the penalty associated with the climb constraint was much larger for the conventional configuration.

The takeoff rotation constraint, introduced in problem 4, increased both the tail area and the DOC slightly for the joined wing. This constraint leads to tail sizes for the conventional configuration that are smaller than those of current production aircraft designed for similar missions. Control authority at maximum lift, effects of tail ice, landing maneuvers, and other constraints also affect the tail size. To avoid the complexity and computational cost associated with including these extra constraints, a 225 ft^2 lower bound on tail area was imposed in addition to the takeoff rotation constraint. As seen in Table 1, this lower bound set the tail area for the conventional configuration.

Designing joined-wing tails to avoid a buckling instability increases the DOC by about 4%. Since a fully stressed design method forms the basis for the structural design used in this study, it might be worthwhile to consider this design issue in more detail. As noted by Petiau et al.,[26] a fully stressed design is not always minimum weight. The indeterminate nature of the joined-wing structure makes it a likely candidate for other structural design methods.

Modifications to flap span, elevator span, wing sweep, and fuel tank arrangement were investigated in an attempt to improve the joined wing's takeoff performance. An extra fuel tank placed in the tail and used to trim at the aft-most c.g. had the most significant impact on joined-wing performance. Taking off at aft c.g. simply reduced the tail download required to trim, and increased aircraft maximum lift. Increasing wing sweep also reduced the tail downloads, but only for wings with relatively short flap spans. At fixed static margin, increasing wing sweep moves the inboard wing section forward and reduces nose-down pitching moment, particularly when inboard flaps are deflected. A study of flap and elevator span indicated that increasing the flap span and decreasing the elevator span produced a better joined wing than increasing the sweep of a wing with 50% span flaps. A more exhaustive study of wing sweep, flap span, and elevator span might show further improvements in joined-wing performance.

The relative importance of each of the constraints was investigated for both conventional and joined-wing transports with a flap-to-wing span ratio of 0.7, an elevator-to-wing span ratio of 0.4, a wing sweep of 30 deg, and a fuel tank in the tail for trim. Figure 13 shows that the takeoff field length constraint is still dominant for joined wings. However, the effect of this constraint has been reduced enough to produce joined-wing transports that are 2% less expensive to operate when the climb gradient and takeoff rotation constraints are included. The penalty in DOC due to buckling from problem 4 to 5 in Fig. 13 is 5.3%. Even though this increase in DOC is larger than that shown in Fig. 12, the increase in DOC when compared with a similarly designed conventional configuration has been reduced from 4.8 to 3.2%. The columns labeled Best and case 3 in Table 1 show the details of aircraft designed for problem 5 and a relative comparison with the reference conventional design.

The increase in penalty caused by the buckling constraint is most likely due to the increase in tail sweep (see Table 1). Increasing the tail sweep increases the compressive tail loads

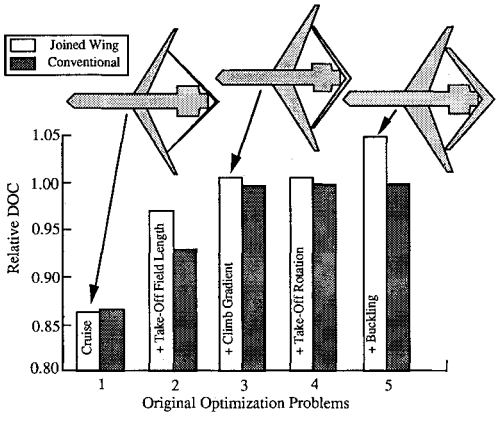

Fig. 12 Effect of constraints on joined-wing and conventional transports. All problems include constraints on range, trim, stability, cruise thrust, and landing field length.

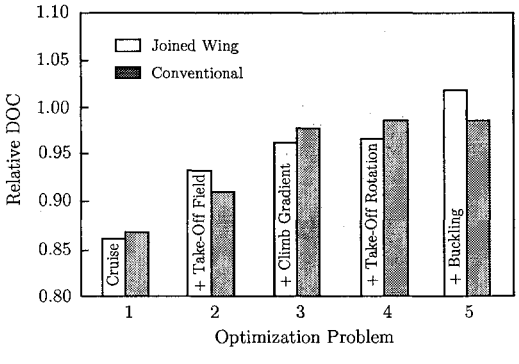

Fig. 13 Effect of constraints on joined-wing and conventional transports, with increased flap span and a tail tank for trim. All problems include constraints on range, trim, stability, cruise thrust, and landing field length.

caused by in-plane wing loads, and decreases the tail's ability to brace the wing. Any design change that reduces tail sweep is likely to improve joined-wing performance.

Conclusions

The results of this study demonstrate the usefulness of numerical optimization as an aircraft design tool and indicate that joined wings have overall performance characteristics similar to conventional transports. Successful, reliable application of numerical optimization to aircraft design depended on the details of the aerodynamic modeling and the smoothness of the problem functions. Takeoff field length and horizontal-tail buckling represented the most critical design constraints for joined wings. A wing sweep of 30 deg and a static margin of 0.2, produced joined wings that were 4.8% more expensive to operate than a comparable T-tail transport designed for the same medium-range transport mission. A significant increase in cost was caused by the joined wing's inability to generate maximum lift in takeoff configuration. Increasing the flap span, decreasing the elevator span, and using a tail tank to trim at aft c.g. led to a joined-wing that saved 2% in DOC before the buckling constraint was considered. Including a buckling constraint increased the DOC by 5.3% and led to a design that cost 3.2% more to operate than the conventional configuration. This quantitative comparison between joined-wing and conventional aircraft applies to the medium-range transport mission considered in this study. Joined-wings that carry payloads that allow for a reduction in tail sweep and that reduce the influence of tail download on maximum lift may perform better than a conventional configuration. The design tools developed for this study can be used to evaluate joined wings for different missions as well as the optimization of other aircraft configurations.

References

[1]Cone, C. D., Jr., "The Theory of Induced Lift and Minimum Induced Drag of Nonplanar Lifting Systems," NASA TR R-139, Feb. 1962.

[2]Wolkovitch, J., "Joined-Wing Aircraft," U.S. Patent 3942747, March, 1976.

[3]Wolkovitch, J., "The Joined Wing: An Overview," *Journal of Aircraft*, Vol. 23, No. 3, 1986, pp. 161–178.

[4]Miura, H., Shyu, A., and Wolkovitch, J., "Parametric Weight Evaluation of Joined Wings by Structural Optimization," *Journal of Aircraft*, Vol. 25, No. 12, 1988, pp. 1142–1149.

[5]Samuels, M. F., "Structural Weight Comparison of a Joined Wing and a Conventional Wing," *Journal of Aircraft*, Vol. 19, No. 6, 1982, pp. 485–491.

[6]Hajela, P., "Weight Evaluation of the Joined-Wing Configuration," NASA CR 166592, June 1984.

[7]Letcher, J., "V-Wings and Diamond-Ring Wings of Minimum Induced Drag," *Journal of Aircraft*, Vol. 9, No. 8, 1972, pp. 485–491.

[8]Kroo, I. M., Gallman, J. W., and Smith S. C., "Aerodynamic and Structural Studies of Joined-Wing Aircraft," *Journal of Aircraft*, Vol. 28, No. 1, 1991, pp. 74–81.

[9]De Filippo, R., "Aircraft Synthesis Using Numerical Optimization Methodology," AIAA Paper 83-2458, Oct. 1983.

[10]Galloway, T., and Waters, M., "Computer Aided Parametric Analysis for General Aviation Aircraft," Society of Automotive Engineers Paper 730332, April 1973.

[11]Kroo, I. M., "A Discrete Vortex Weissenger Method for Rapid Analysis of Lifting Surfaces," Desktop Aeronautics, Stanford, CA, Aug. 1987.

[12]Beltramo, M. N., Trapp, D. L., Kimoto, B. W., and Marsh, D. P., "Parametric Study of Transport Aircraft Systems Cost and Weight," NASA CR 151970, April 1977.

[13]Gill, P. E., Murray, W., Saunders, M. A., and Wright, M. H., "User's Guide for NPSOL (Version 4.0): A Fortran Package for Nonlinear Programming," Dept. of Operations Research, TR SOL 86-2, Stanford Univ., Stanford, CA, Jan. 1986.

[14]Hoak, D. E., and Fink, R. D., "USAF Stability and Control DATCOM," Sec. 4.1.3.4 and 6.1.1.3, Flight Control Div., Air Force Flight Dynamics Lab., Wright-Patterson AFB, OH, April 1978.

[15]Shevell, R. S., and Kroo, I., "Introduction to Aircraft Design Synthesis and Analysis," Course Notes, Dept. of Aeronautics and Astronautics, Stanford Univ., Stanford, CA, 1990.

[16]von Kármán, T., "Turbulence and Skin Friction," *Journal of the Aeronautical Sciences*, Vol. 1, No. 1, 1934, pp. 1–20.

[17]Shevell, R. S., *Fundamentals of Flight*, Prentice-Hall, Englewood Cliffs, NJ, 1983.

[18]McGeer, T., and Shevell, R., "A Method for Estimating the Compressibility Drag of an Airplane," Dept. of Aeronautics and Astronautics, SUDAAR 535, Stanford Univ., Stanford, CA, Jan. 1983.

[19]O'Banion, J., Jhou, J., Stearman, R., and Smith, S., "A Study of Joint Fixativity in a Joined-Wing Configuration," Society of Automotive Engineers TP-871048, April 1987.

[20]Hajela, P., "Reduced Complexity Structural Modeling for Automated Airframe Synthesis," NASA CR 177440, May 1987.

[21]"Estimated Aerodynamic Data for Stability and Control Calculations Model DC-9-30 Jet Transport," Douglas Aircraft Co., Rept. LB-32322, Long Beach, CA, May 1966, revised Jan. 1967.

[22]"ATA Standard Method of Estimating Comparative Operating Costs of Turbine Powered Aircraft," Air Transport Association of America, Washington, DC, Dec. 1967.

[23]Gill, P. E., Murray, W., and Wright, M. H., *Practical Optimization*, Academic Press, New York, 1981.

[24]Hamming, R. W., *Numerical Methods for Scientists and Engineers*, McGraw-Hill, New York, 1973.

[25]Torenbeek, E., *Synthesis of Subsonic Airplane Design*, Delft Univ. Press and Martinus Nijhoff, Holland, 1982.

[26]Petiau, C., and Lecina, G., "Elements Finis et Optimisation des Structures Aeronautiques," *AGARD Conference Proceedings No. 280—The Use of Computers as a Design Tool*, Neubiberg, Germany, Sept. 1979, pp. 23-1–23-16.